THE ASTROPHYSICAL JOURNAL, 462:296–308, 1996 May 1

ON THE DUST-TO-GAS RATIO AND LARGE PARTICLES IN THE INTERSTELLAR MEDIUM

SANG-HEE KIM
Korea Astronomy Observatory, 36-1, Whaamdong Yuseonggu, Daejon, 305-348, Korea; shkim@hanul.issa.re.kr
AND
P. G. MARTIN
Canadian Institute for Theoretical Astrophysics, University of Toronto, Toronto, Ontario, Canada M5S 3H8; pgmartin@cita.utoronto.ca
Received 1995 July 19; accepted 1995 October 24

ABSTRACT

A comparison of mass (or size) distributions of interstellar dust particles in various environments (from diffuse to dense), as determined from interstellar extinction and linear polarization curves, shows that for dense (dark) clouds with higher R_V and λ_{max} than typical of the diffuse interstellar medium the relative number of small particles is greatly diminished, whereas the shape of the mass distribution at the large size end (where much of the mass is) is much the same. This appears to be consistent with evolution of interstellar dust particles in dense clouds by aggregation involving small particles; there is only modest evolution of the larger particles. There is some evidence for dark cloud lines of sight with lower than average extinction per unit mass of gas (e.g., A_V/N_H is one measure). With specific application to the ρ Oph line of sight, we show quantitatively that this demands the existence of particles much larger than usually contemplated (10 μm). Large particles have low extinction efficiencies per unit volume in the optical and fairly neutral extinction with wavelength and so can lock up a lot of mass fairly inconspicuously. Producing such particles requires much more aggressive aggregation, with large particles sticking to one another. While our analysis is based on specific grain models, an instructive Kramers-Kronig treatment illustrated by these models suggests that our conclusions are robust.

Subject headings: dust, extinction — ISM: abundances

1. INTRODUCTION

Mass (or size) distributions of interstellar dust particles for various environments (from diffuse to dense) have been determined from the interstellar extinction (Kim, Martin, & Hendry 1994, hereafter Paper I) and linear polarization curves (Kim & Martin 1994, 1995). A comparison of the mass distributions for dense (dark) clouds with higher R_V and λ_{max} with those typical of the diffuse interstellar medium showed that in the dense clouds the relative number of small particles is greatly diminished, whereas the *shape* of the mass distribution at the large size end (where much of the mass is) is much the same (see § 2.1). This appears to be consistent with evolution of interstellar dust particles in dense clouds by aggregation rather than by accretion. Interesting questions arise. Is the dust to gas ratio (by mass) the same in these different environments? This is related to cosmic abundances and changes in gas phase depletion from the diffuse medium (where depletion is already high for limiting species like Si, Mg, and Fe) to denser clouds (see Sophia, Cardelli, & Savage 1994 for a contemporary discussion). How does the amount of extinction per unit mass of gas (e.g., A_V/N_H is one measure) vary? This is related to the distribution of dust mass, since different sizes have different extinction efficiencies per unit dust mass. Large particles have low extinction efficiencies per unit volume in the optical and fairly neutral extinction with wavelength and so could lock up a lot of mass fairly inconspicuously.

In § 2 we present the mass distribution of interstellar particles determined from various parameterized extinction curves, with the aim of maximizing A_V/N_H for a given amount of material. The pressing problem of the amount of C available for grains is addressed in § 2.3. In § 3 we discuss A_V/N_H values gathered from various sources. Jura (1980) has presented evidence for aggregation based on a lower value of A_V/N_H observed toward ρ Oph than on lines of sight through the diffuse interstellar medium. This important and widely cited result is revisited and analyzed here (§§ 3, 4, and 6). Grain mass distributions determined from the extinction curve toward ρ Oph are presented in § 4, revealing the need for very large particles (10 μm). The evolution of the grain surface area is examined in § 4.1. Potential independent observational constraints on large particles are discussed in § 5.

A_V/N_H is not necessarily the best measure of the dust to gas ratio. Purcell (1969) has suggested a potentially powerful alternative based on application of the Kramers-Kronig relations to the interstellar extinction curve. Despite limitations of this approach, as demonstrated in § 6, a powerful application can be made to cases like ρ Oph.

2. MASS DISTRIBUTIONS WHICH MAXIMIZE A_V/N_H

Extinction curves have two basic properties to be explained: the shape (or wavelength dependence), which can be parameterized in terms of R_V (Cardelli, Clayton, & Mathis 1989, hereafter CCM; we shall be interested in the representative sample $R_V = 2.7$, 3.1, 4.2, and 5.3), and absolute value (or normalization), which is often described by A_V/N_H. In this section we seek the maximum amount of extinction, A_V/N_H, that can be produced by a given amount of condensed interstellar material (in the nominal form of silicates and graphite here) that is distributed in grains of different masses so as to explain the overall shape of the extinction curve.

From Bohlin, Savage, & Drake (1978, hereafter BSD), the abundance constraint for the case of the diffuse interstellar

medium, where $R_V = 3.1$, can be expressed as (see also § 3)

$$A_V/N_H = 0.53 \times 10^{-21} \text{ mag cm}^2 . \quad (1)$$

Setting this as a target normalization, we then find how little material is required in the mass distribution of the grains. For extinction curves of different shapes (R_V), we fix this amount of material and find, by redistributing the material among grains of different masses, how large A_V/N_H can be.

As in Paper I we use a maximum entropy analysis to determine the mass distribution objectively. In anticipation of the discussion below of the large end of the mass distribution, we extended the size range to ~ 90 μm with the same bin size. The shape of the default mass distribution used in the analysis is a power law with an exponential decay (PED) above some size a_b,

$$m(a) \propto a^{-\gamma} \exp(-a/a_b) . \quad (2)$$

2.1. *Minimizing the Mass*

As demonstrated in Paper I, the size range that can be constrained given data over the finite wavelength range 0.1 to 5.1 μm is ~ 0.02 to 1.0 μm. As shown below, if a large value of a_b is chosen, it is possible for the maximum entropy solution to have a significant mass of large particles in the unconstrained region (see also § 4). The visual extinction per unit mass is less for large particle sizes ($\propto 1/a$ for sufficiently large sizes), thus lowering A_V/N_H. Desiring the opposite, we concentrated first on lower a_b. If the value is set too low, then the default solution will produce too little differential extinction through the infrared and visual, and the solution will correct the distribution accordingly. The solutions shown in Figure 1 all have the same $a_b = 0.2$ μm and $\gamma = 0.2$ in the default distribution to emphasize differential effects as the shape of the extinction curve changes with R_V.

As in Paper I, for $R_V = 3.1$ the solution uses Si/H $= 3.4 \times 10^{-5}$ (34 ppM) or 95% of the cosmically available Si consistent with depletion studies of the diffuse interstellar medium; comparable amounts of Mg and Fe are also needed. The actual form of silicate might not be quite like we adopted ("astronomical silicate" from Draine & Lee 1984); more complex structure might exist in glassy silicates (e.g., Martin 1995), and there might be various distinct oxides of Si, Mg, and Fe (Sophia et al. 1994). Nevertheless we feel that the mass of these elements in grains and the extinction produced is fairly robust.

The cosmic abundance and depletion of C is more controversial (see § 2.3), and so consistent with the goals of this subsection we aimed to minimize the amount of C required. Using a graphite composition, this minimum is C/H $\simeq 3.1 \times 10^{-4}$ (310 ppM). The dust to H mass ratio is 0.0095 (silicate 0.00573 and graphite 0.00374; the silicate to graphite mass ratio is 1.53, whereas the silicate to graphite volume ratio is 1.05).

The above solution concentrated on fairly low values of a_b. We also examined defaults that would allow substantial numbers of large particles. One example is shown in Figure 2 for $a_b = 10$ μm; the mass distributions are for $R_V = 3.1$ and the standard A_V/N_H, and $\gamma = 0.8$. For comparison, the model from Figure 1 ($\gamma = 0.2$, $a_b = 0.2$ μm) is reproduced. The mass distributions for small sizes look similar, because of the choice of different values of γ. At intermediate sizes (0.1 μm) there is a slight redistribution in size and between compositions. There is a tail in the silicate distribution to large sizes beyond ~ 0.5 μm, following the default. At the same time, the hump in the graphite distribution at 0.7 μm (above the default for $a_b = 0.2$ μm) is no longer necessary (to fit the infrared extinction), being redistributed among intermediate- to large-size particles. Consistent with the above, we find that models with a_b somewhat larger for the silicate component compared to that for graphite are quite acceptable (§ 2.3).

In these distributions for high a_b there is a modest number of large particles. But the number is limited by the abundance constraint and the requirement to produce the target A_V/N_H. About 19% of the silicate mass is in sizes greater than 0.5 μm, and $\sim 5\%$ for graphite. Together they

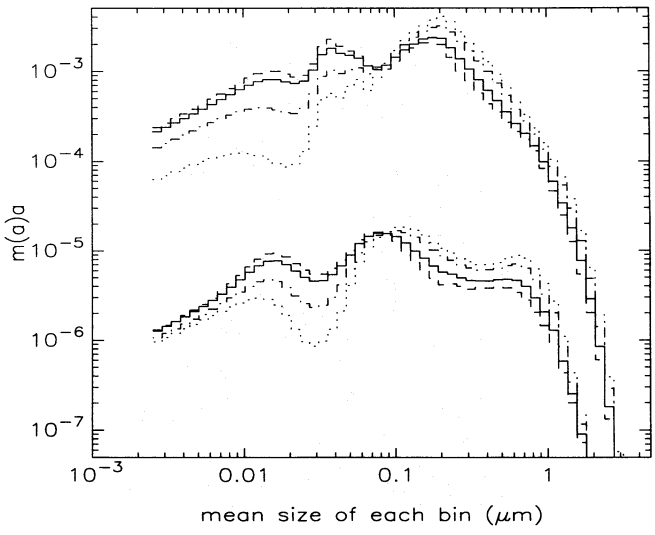

FIG. 1.—Mass distributions, expressed relative to the mass of hydrogen, determined from parameterized extinction curves for different R_V (*dashed curve*: $R_V = 2.7$; *solid curve*: $R_V = 3.1$; *dot-dashed curve*: $R_V = 4.2$; *dotted curve*: $R_V = 5.3$). Upper histograms for silicate and lower ones for graphite (scaled down by a factor 100 for clarity). The same amount of mass is used independently of R_V.

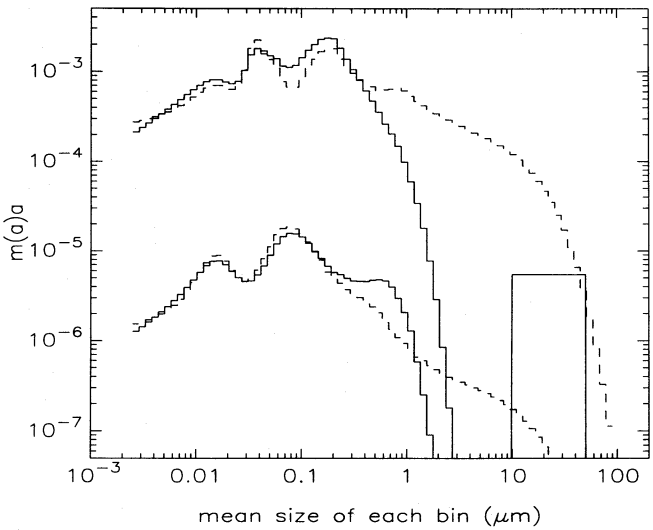

FIG. 2.—Same as Fig. 1, except for $R_V = 3.1$ with different MEM defaults. *Solid bin*: $\gamma = 0.2$ and $a_b = 0.2$ μm (Fig. 1). *Dashed curve*: $\gamma = 0.8$ and $a_b = 10$ μm. The solid block centered at 30 μm represents the amount of large C particles suggested by Rowan-Robinson (1992) (scaled down by a factor 100 for comparison with the graphite histograms).

contribute a gray optical extinction amounting to only 1.5% of the total extinction at V.

In a composite model of interstellar extinction and submillimeter emission, Rowan-Robinson (1992) included a significant quantity of large (30 μm) C grains (amorphous carbon). The suggested amount, shown for comparison with the graphite mass distributions in Figure 2, is clearly much in excess of the MEM models. These additional grains would increase the (gray) optical extinction by 0.3% (at V) while increasing the C/H budget from 310 to 360 ppM. Therefore, if required for the submillimeter emission, these grains ought to be included self-consistently in our MEM modeling.

2.2. *Variation with R_V*

For extinction curves with higher values of R_V we found that solutions with $a_b = 0.2$ μm for the same A_V/N_H normalization as in equation (1) did not use up the amount of material determined above for $R_V = 3.1$. Consequently we raised A_V/N_H in small steps until, in an iterative fashion, we found a solution that did. Compared to equation (1), these had A_V/N_H increased by 1.12 and 1.2 for $R_V = 4.2$ and 5.3, respectively. In the same spirit, the solution for the case of $R_V = 2.7$ had a lower A_V/N_H by a factor 0.93.

When R_V is increased for the same A_V/N_H, the relative number of large particles can grow. The mass can be accommodated without increasing A_V/N_H but appears as a large bulge above the defaults near 10 μm. This size is sufficiently large so as not to produce appreciable optical extinction. As A_V/N_H is increased (by a factor 1.2 for $R_V = 5.3$) this bulge disappears; solutions for higher A_V/N_H are not satisfactory.

The conclusion is that for models in which the total mass of grains is conserved (and kept to a minimum determined for $R_V = 3.1$), the maximum A_V/N_H actually increases slightly with R_V. The reason for this can be understood by differential comparison of the resultant maximum entropy mass distributions shown in Figure 1 (likewise for the higher a_b solutions). First, the constraint provided by the common shape of the infrared extinction curve for any R_V causes a turnover in the shape of the mass distribution [specifically $m(a)a$] near $a = 0.1$ μm; there is actually a small shift in the position of the peak as R_V increases, by a factor $\sim 2^{1/3}$ (corresponding to a mass increase by a factor of 2) over the range $R_V = 3.1$–5.3. But in any case, large numbers of even larger particles are precluded by the choice of a_b being small or a smooth extrapolation along the default. Second, there is a great reduction in the relative number of small grains with $a < 0.05$ μm as R_V increases. Then, since mass is conserved, this mass is redistributed among larger particles near the peak of the distribution. The particle size at the peak is fairly optimal for producing visual extinction, and so A_V/N_H increases with R_V.

The physical interpretation of these mass distributions as an evolutionary sequence would be that in dense regions aggregation of small with large particles is efficient within a cloud lifetime, whereas large particle aggregation is not (see discussion in Paper I). Our polarization analyses reach similar conclusions (Kim & Martin 1994, 1995). A comprehensive study of dust properties in the ρ Oph cloud is presented by Vrba, Coyne, & Tapia (1993); evidence for modest grain size evolution is found to be consistent with turbulence-driven aggregation.

It should be emphasized that the gas phase abundances or amounts of depletion of major species are not as well known in dense regions of the interstellar medium (but see Snow & Jenkins 1980 for the ρ Oph cloud). Since eventually ices are observed to have formed, it seems unlikely that the depletion is any less than in the diffuse medium. Ices can add another 10% to the mass of material (Jenniskens et al. 1993) but would not increase the grain sizes substantially if distributed as thin layers over all grains. This would reinforce the increase of A_V/N_H with R_V found above. A further increase in A_V/N_H would be possible by depleting the rest of the Si, but since this was already 95% depleted, the potential increase is not substantial; the silicate model also incorporated most of the Fe and Mg, and so little increase based on these elements is possible. Deposition of C-rich materials (amorphous carbon, HAC, organic refractories) is of greater potential for increasing A_V/N_H, given the gas phase C/H ratio of 140 ppM in the diffuse interstellar medium (Cardelli et al. 1996); this option is to be constrained ultimately by the amount of C that remains in CO or atomic form. Mathis (1996) concluded that there was in fact no further depletion of C (see also § 2.3).

2.3. *The* C/H *Crisis*

An issue that we can address somewhat objectively with our MEM analysis is how much C is required in grains to explain the observed extinction. For the models for $R_V = 3.1$ in § 2.1 that put C in graphite this requirement is C/H $\sim$ 310 ppM. The Mathis, Rumpl, & Nordsieck (1977) and Draine & Lee (1984) models also required $\sim$300 ppM.

To lower the required C/H in the grains for $R_V = 3.1$ we experimented with increasing a_b for the silicate default while lowering that for graphite. By slight modification of the relative weights of infrared and ultraviolet data and a slight increase in the allowed χ^2 of the fit, this approach met with modest success. For example, with a_b(silicate) = 0.3 μm and a_b(graphite) = 0.1 μm, C/H can be reduced to $\sim$260 ppM. The carbon requirement depends somewhat on the carbonaceous material adopted for the basic building blocks. C/H can be lowered by having C mostly in amorphous carbon particles, with the number of *small* graphite particles the minimum necessary to explain the 2175 Å extinction bump (Paper I). For the case with $a_b = 0.2$ μm in common for silicate and amorphous carbon, C/H is reduced slightly to 270 ppM; of this, $\sim$80 ppM is required in the small graphite particles, consistent with other estimates. Combined with tinkering with a_b as above, C/H can be lowered to 240 ppM.

Comprehensive models must explain the near-infrared emission in the "unidentified infrared bands" (UIBs) and extended red emission (ERE) in reflection nebulae; as reviewed by Mathis (1996), the required C/H is perhaps 30 ppM with considerable uncertainty. We emphasize that this amount does not have to be added to the (minimum) 240 ppM just cited; the UIB and ERE emission is powered by (far) ultraviolet absorption, and the total far-ultraviolet extinction is already accounted for in our grain model (whether we have the precise C-bearing species is another question). Alternatively, subtracting the small-graphite and UIB/ERE carbon requirements ($\sim$110 ppM) from the total, we need a minimum of 130 ppM in some additional form of carbon grains (160–200 ppM would obviously be more comfortable).

Other models that have been developed use similar amounts of C. That of Rowan-Robinson (1992) uses 210 ppM to explain the extinction, about half in graphite and

half in amorphous carbon of uncertain optical properties, plus 60 ppM in large 30 μm grains. Enhanced extinction efficiency by amorphous carbon and HAC is proposed by Duley, Jones, & Williams (1989) and still C/H = 190 ppM (this would be higher except that the 2175 Å extinction bump is explained by silicates). In models where carbon is largely in organic refractory mantles, the requirement is 260 ppM, or perhaps as low as 190 ppM for residues with enhanced extinction efficiency (Chlewicki & Greenberg 1990).

The question arises whether composite grains (silicate, graphite, amorphous carbon material, and possibly vacuum all within one particle) could ease the abundance requirement. One problem is exactly how to treat the electromagnetic scattering by the composite grains. Models calculated using the Bruggeman mixing rule to obtain an effective refractive index (Mathis & Whiffen 1989) consume C/H $\sim$ 300 ppM in grains. Independent models have been carried out using the Maxwell-Garnett mixing rule (Mathis 1996); models with C/H $\sim$ 260–360 ppM in grains (lower values require more silicate) might be satisfactory (60 ppM of this in small graphite), but with C/H as small as 220 ppM the extinction is surely severely underestimated.

Comprehensive models must also explain the albedo of interstellar grains (Paper I, § 5.1). In our models, and in all of the other different models mentioned above, the *visual* albedo is lowered from near unity (for "silicates") toward the observed value by means of the carbon content in grains of size $\sim$0.1 μm (not by the small-graphite and UIB/ERE components); this provides independent support for the minimum 130 ppM in such grains.

Knowledge of the gas phase abundance of C in the diffuse interstellar medium has been greatly improved recently by Cardelli et al. (1996) using the *Hubble Space Telescope*. They find C/H to be 140 $\pm$ 20 ppM, and so C has not been entirely depleted. In molecular clouds the situation is less well studied, but there are new observations of interest. For example, Lacy et al. (1994) measured the CO and H_2 abundances toward NGC 2024 IRS 2 using infrared absorption lines, finding C/H = 130 ppM (with a factor 2 uncertainty); they found a lower limit of 100 ppM toward NGC 2264. These ratios are perhaps higher than previously thought and comparable to those for the diffuse medium. In a broad region surrounding NGC 2024 Jaffe et al. (1994) find that the column densities of C^+, from [C II] 157 μm observations, and CO, based on ^{13}CO, are comparable. Lacy et al. interpret this as another 130 ppM for C^+; this would be curious, since dust would have to have been destroyed compared to the diffuse interstellar medium to liberate this extra C (also only one-third of the solar C/H would be available for grains toward NGC 2024). However, this interpretation is probably in error, because the [C II] emission likely arises from the outer regions of photodissociation regions where the hydrogen is largely atomic (Hollenbach, Takahashi, & Tielens 1991) and hence undetected in a census using only H_2 (the CO would arise in the region where hydrogen is molecular).

The next matter of interest is the solar abundance of C, often adopted as the "cosmic" (total interstellar) value. In his review Mathis (1996) adopts C/H = 400 $\pm$ 50 ppM from Grevesse et al. (1991), whereas Cardelli et al. (1996) adopt 350 $\pm$ 40 ppM from Grevesse & Noels (1993). The higher value minus the interstellar gas phase ratio leaves 260 ppM from which to form carbon dust; this appears to be compatible with the grain models discussed above. However, with the lower value there remain only 210 ppM for dust, leaving the models in some jeopardy. In either case, there is no excess C to squander on unobserved (in the visual) large grains as envisioned by Rowan-Robinson (1992).

For solar O/H = 740 ppM (Grevesse & Noels 1993), there is a case of "missing O," unaccounted for in interstellar atoms, molecules, and probably dust (Cardelli et al. 1996). Meyer et al. (1994) and Cardelli et al. (1996) argue that cosmic O/H is instead closer to $\frac{2}{3}$ the solar value, close to the median value deduced for Galactic B stars. Then there is no missing O.

Cardelli et al. (1996) observe that C/H in Galactic B stars is also $\sim\frac{2}{3}$ solar; furthermore, if the C/O ratio is a constant, independent of the absolute level of C/H, then the cosmic C/H ratio should also be lower, $\sim$240 ppM. If this is the case, there is clearly a crisis for models of interstellar extinction trying to make do with a meager ration of C/H $\sim$ 100 ppM. While this is enough for small graphite grains for the 2175 Å extinction bump and for the UIB/ERE carriers, there is no leeway for an important C contribution to the general extinction and a lowering of the albedo. General arguments based on the Kramers-Kronig relations (§ 6) suggest that this extinction contribution must somehow be restored or replaced. Mathis (1996) reflects on the "somewhat indirect reasoning" by which one arrives at the cosmic abundances and points out that one must also understand the vexing question of abundances in H II regions to have a comprehensive picture. Resolving these many interrelated issues is beyond the focus of this paper. It is not inconceivable that we are not being clever enough with the grain models, but at this point we are inclined to suggest that the interpretation of there being a subsolar cosmic C/H ratio must somehow have gone wrong.

3. A_V/N_H FOR VARIOUS ENVIRONMENTS

The question addressed in this section is "what observational evidence is there on how A_V/N_H varies with environment?" or to the extent that environmental changes are characterized by R_V, with R_V?

Generally the value N_H includes atomic and molecular forms (H I plus $2H_2$). BSD presented interstellar column densities N(H I) toward 100 stars from the *Copernicus* satellite and combined these with *Copernicus* data on $N(H_2)$ from Savage et al. (1977) to form N_H for 96 stars. They found a good correlation between N_H and $E(B-V)$ (typical scatter of only 30% about the mean line; see Fig. 3), reported as $N_H/E(B-V) = 5.8 \times 10^{21}$ cm^{-2} mag^{-1}, a commonly adopted representative value for the diffuse interstellar medium. Combining this with $R_V = 3.1$ gives us the A_V/N_H cited in equation (1).

Shull & van Steenberg (1985, hereafter SvS) used *IUE* high-dispersion spectra to measure N(H I) for 205 stars, extending the range to higher $E(B-V)$ (or N_H). For 78 stars in common with *Copernicus* data, the agreement of the N(H I) column densities is generally good; the largest discrepancy is unfortunately for ρ Oph [log N(H I) = 21.60 $\pm$ 0.10 vs. 21.85 $\pm$ 0.15 in BSD]. Similarly, Diplas & Savage (1994a) measured a total of 554 stars, including a refined analysis of 263 stars studied earlier by SvS and Savage & Massa (1987). The agreement was good (0.13 dex); they also found log N(H I) = 21.63 for ρ Oph. However, after assessment of the contamination by stellar Lyα absorption, 161 stars were rejected by Diplas & Savage

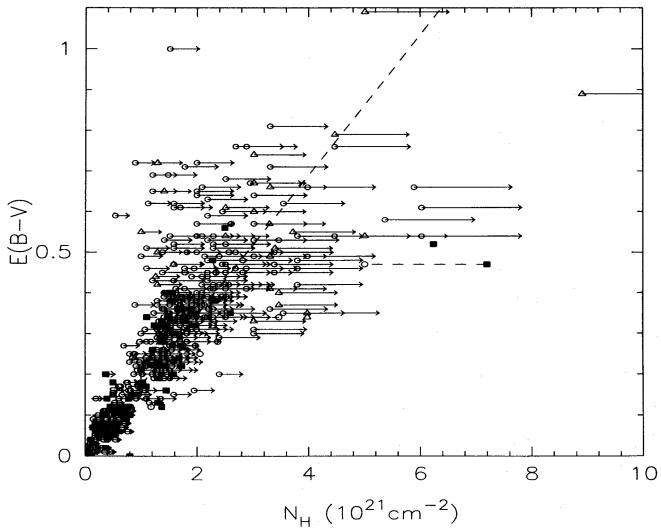

FIG. 3.—$E(B-V)$ vs. total hydrogen column density N_H. The diagonal line is the average relation for the diffuse interstellar medium determined by BSD. Solid squares represent the data from BSD, open circles from Diplas & Savage (1994a), and open triangles from Fitzpatrick & Massa (1990). Broken lines connect cases where a different column density for the same star has been measured by different authors. Solid lines with arrows connect column densities of atomic hydrogen with approximately determined total hydrogen (*see text*).

as unreliable, leaving 393 stars for our plots (their Table 1). We combined the Diplas & Savage values of N(H I) with data on $N(H_2)$ from Savage et al. (1977) where possible and plotted the data in Figure 3; this does not add much to what is already shown for BSD, except for ρ Oph. For the remaining stars, we estimated $N(H_2)$ using the average behavior of $f = 2N(H_2)/[2N(H_2) + N(\text{H I})]$ discussed by Savage et al. For the more interesting stars with $E(B-V) > 0.2$, $f \sim 0.22$ but with a factor 3 scatter either way; thus $2N(H_2)/N(\text{H I}) \sim 0.28$ but ranges from 0.1 to 2 or more. Data for these stars are also presented in Figure 3, using N(H I) (lower bound) with an arrow to the estimated N_H.

Fitzpatrick & Massa (1990) used *IUE* low dispersion spectra to measure N(H I) for 45 stars. This study was focused on unusual environments (dark clouds, reflection nebulae, H II regions) and so extends the sample to a larger range of R_V. For cases of overlap with high dispersion measurements, the agreement with SvS and Diplas & Savage is usually good. But a measurement of θ^1 Ori C ($R_V = 5.5$) by Savage et al. (shown as solid square like BSD) is much lower than reported by Fitzpatrick & Massa (Fig. 3: $E(B-V) = 0.34$, $N_H = 4 \times 10^{21}$ cm^{-2}); the latter is supported by Diplas & Savage ($N_H = 3.5 \times 10^{21}$ cm^{-2}). Data for 31 stars for which there were no previous measurements are plotted in Figure 3 in the same way as the Diplas & Savage data for which there were no $N(H_2)$ measurements.

For low reddening [$E(B-V) < 0.3$] for which unaccounted-for H_2 should not be a problem, Diplas & Savage (1994b) find a slope 1.8×10^{-22} mag cm^2, close to the quoted BSD value 1.7×10^{-22} mag cm^2 (diagonal line in Fig. 3). However, they point out that for lines of sight with relatively high values of mean density ($n_H > 1.5$ cm^{-3}) the slope is somewhat lower (1.3×10^{-22} mag cm^2). For these points below the diagonal line, the deficit would only be enhanced by allowance for undetected $N(H_2)$. Thus there are other stars in more dense regions for which, like for ρ Oph, there is a deficiency of $E(B-V)$, pointing to some modification of the dust.

A more relevant quantity is A_V/N_H, which involves the absolute rather than the differential extinction; it is possible that a low value of $E(B-V)$ can be compensated by a high value of R_V, as BSD noted in connection with ρ Oph. Therefore, for the subset of stars with known R_V (see CCM) we plotted A_V versus N_H in Figure 4. For stars with unknown R_V we used the mean relation $R_V = -0.29 + 6.67\lambda_{max}$ from Clayton & Mathis (1988) to estimate R_V (λ_{max} is the wavelength of maximum interstellar linear polarization; see Serkowski, Mathewson, & Ford 1975); this adds a few more points to Figure 4. The diagonal line is equation (1). There are still some stars below the line but many have moved closer (or above), for example HD 164740 (Herschel 36), which has $E(B-V) = 0.89$, $R_V = 5.3$, and $N(\text{H I}) = 8.9 \times 10^{21}$ cm^{-2}.

More directly to the issue here of systematic grain evolution, we show A_V/N_H versus R_V in Figure 5. In this logarithmic form the arrows for stars with unknown $N(H_2)$ are mostly the same length ($\sim$0.1 dex), but the range could be as large as 0.03–0.5 dex; the error in A_V/N_H from N(H I) is typically 0.1 dex as well. The solid line gives the expected maximum value obtained by the analysis in § 2, whereas the dashed line is equation (1). Most of the BSD stars are excluded individually, having undetermined R_V presumably near 3.1; they would appear near the intersection of the two lines, scattering above and below the dashed line by $\sim$0.1 dex.

The case for systematic differences in A_V/N_H as a function of R_V is not very strong. For $R_V < 4.4$ the scatter is rather large, consistent with Figure 3 and the observational uncertainty. Among the points with arrows, there appears to be a bias to the high side of the average. Recall from the discussion in § 2 that it is hard to explain A_V/N_H much higher than the average without incorporating in the grains further material, particularly C, beyond that assumed; in denser regions with slightly elevated R_V there could be enhanced depletion, but this is questionable given current evidence

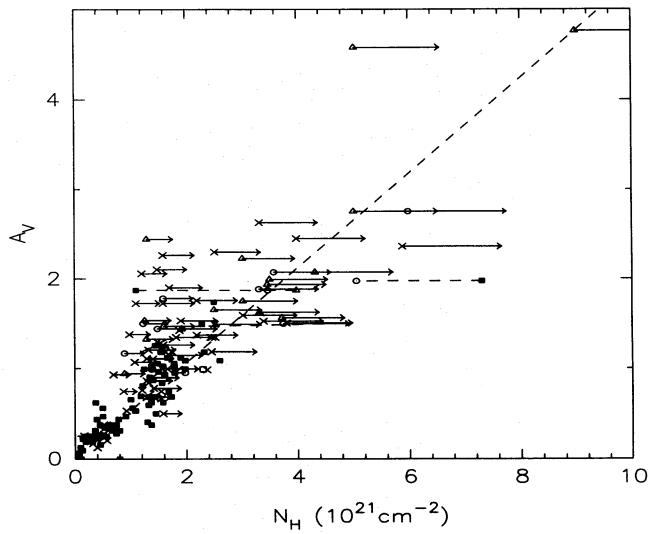

FIG. 4.—Like Fig. 3 but for $A_V = R_V E(B-V)$ for stars with known R_V and for the rest of the BSD data assuming $R_V = 3.1$. Additional data plotted as crosses use an approximate R_V from λ_{max}. Dashed line is eq. (1), the diffuse medium average from BSD and Fig. 3, again assuming $R_V = 3.1$.

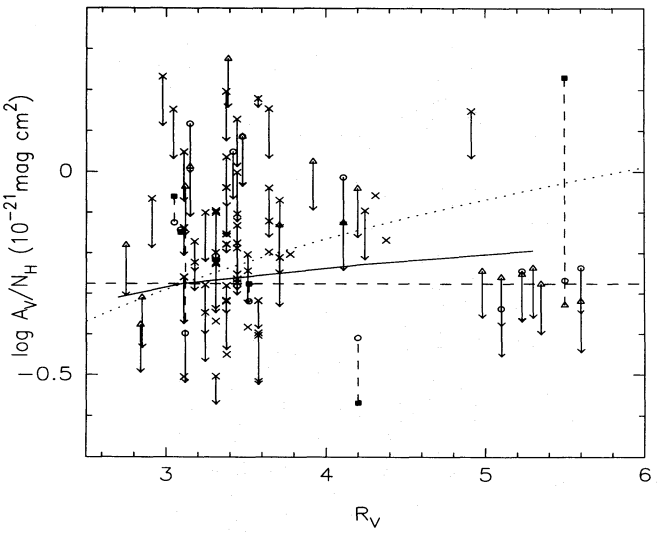

FIG. 5.—Log A_V/N_H vs. R_V for stars in Fig. 3 with known R_V, with same symbols. Additional data plotted as crosses use an approximate R_V from λ_{max}. The solid line is the maximum A_V/N_H for our constant-mass MEM models in Fig. 1. The dashed line is eq. (1), the diffuse medium average. Most BSD data would presumably appear near the intersection of the two lines. The dotted locus shows how a point at this intersection $R_V = 3.1$ would move if R_V were chosen erroneously.

(§ 2.3). On the other hand, denser regions might also have higher f than the assumed average, extending the arrow downward in Figure 5. For example, the highest point in the diagram at $R_V = 3.4$ is for the dark cloud line of sight to HD 73882; a counterexample is the ρ Oph cloud with unusually low f (Snow 1983; Cardelli 1988; § 4.1).

BSD found that $E(B-V)/N_H$ in the line of sight toward ρ Oph was significantly lower than their average, but they noted that this could be offset by a higher value of R_V to yield a more normal dust to gas ratio. However, $R_V = 4.2$, which is really not enough: A_V/N_H is lower than the average by 0.3 dex. This remarkable result (still the lowest point in Fig. 5) was the basis of Jura's (1980) contribution on aggregation in dense regions. As noted above, SvS found a somewhat lower value of N(H I) such that A_V/N_H is only 0.1 dex low and so is indistinguishable from the average within the stated observational uncertainty. Reanalysis of data from *Copernicus* by de Boer et al. (1986) and from *IUE* by Diplas & Savage (1994a) support this higher ratio. On the basis of this star alone, the case is not very convincing. Note also that A_V/N_H of a neighboring star, HD 147889, is $\sim$0.1 dex higher than average ($R_V = 4.2$).

Given the observational errors, perhaps a statistical approach is better. At the highest R_V, the value of A_V/N_H does appear to be lower than average [potentially much lower, depending on $N(H_2)$] and at least statistically definitely lower than the maximum (with no further depletion) that was discussed in § 2. However, five of the seven stars are in Orion, and so establishing how representative this low value is of high R_V lines of sight generally would still benefit from further data.

Such is the evidence for A_V/N_H values lower (or higher) than the average and expected maximum. Perhaps the most remarkable thing is how uniform the value is. The next sections explore the potential implications for aggregation and the abundance of large particles in the mass distribution.

4. ρ OPHIUCHI

Jura's (1980) paper concentrated on the line of sight to ρ Oph A (HD 147933). This is analyzed quantitatively here. The extinction curve used for determining the mass distribution was obtained as follows. For the range 0.2–3 μm^{-1} we used the parameterized CCM extinction curve with $R_V = 4.2$; the CCM curve passes through all the data points except one at 3.5 μm obtained by Carrasco, Strom, & Strom (1973) and another one at 0.33 μm obtained by Serkowski (1968). The Fitzpatrick & Massa (1990) fit for this star is used in the ultraviolet range 3–8.5 μm^{-1}. At higher wavenumbers (up to 10 μm^{-1}), we interpolated the actual data (Green et al. 1992). As mentioned in § 3, A_V/N_H for this line of sight is said to range from 0.42×10^{-21} mag cm^{-2} (SvS) to 0.27×10^{-21} mag cm^{-2} (BSD), with measurements by de Boer et al. (1986) and Diplas & Savage (1994a) supporting the former. These values correspond to 0.79 and 0.51 times the BSD average value in equation (1), or 0.71 and 0.45 times the maximum established for $R_V = 4.2$ in § 2.1 (Fig. 1). We have determined mass distributions considering both A_V/N_H values (the MEM analysis has enough flexibility to provide a good fit to the extinction curve, in contrast to simple power laws considered by Green et al.).

Some results are shown in Figure 6, all using $\gamma = 0.0$. With the SvS value of A_V/N_H and $a_b = 0.2$ μm the solution looks reasonable (*solid curve*) but the total dust to H mass ratio used is 0.0065, as expected, $\sim$70% of the maximum 0.0095 available (about the same silicate to graphite ratio). To give the MEM analysis the flexibility to use up the available mass we increased a_b, finding $a_b = 5$ μm to be about the minimum value. This is shown as the dashed curve (dust to gas ratio 0.0095 as in Fig. 1). With the even lower BSD value of A_V/N_H, it is necessary to increase a_b to 20 μm in order to consume the available mass (*dotted curve*).

As expected, the additional particles required to make up the mass appear in the latter two mass distributions at large sizes where their numbers are quite unconstrained by the

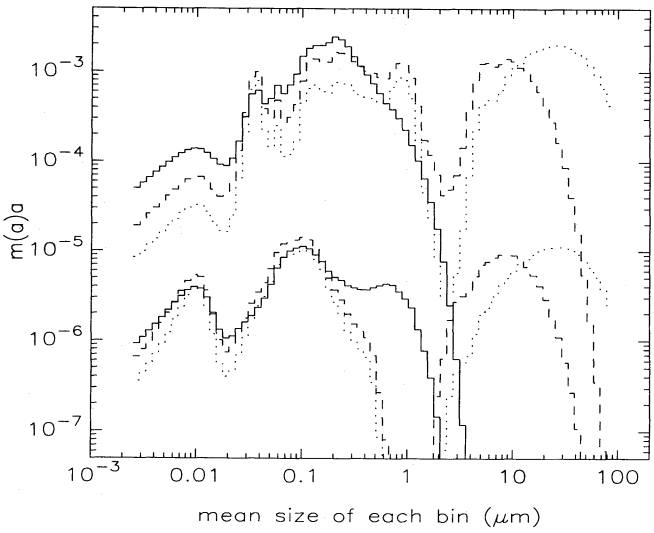

FIG. 6.—Mass distributions like Fig. 1, but for extinction curve of ρ Oph A (HD 147933). Different solutions are for different MEM defaults and choice of A_V/N_H. For all the cases, $\gamma = 0$. *Solid curve*: subnormal A_V/N_H from SvS and $a_b = 0.25$ μm; this does not use up the available mass. *Dashed curve*: A_V/N_H from SvS and $a_b = 5$ μm, the minimum which ensures that all the mass is used. *Dotted curve*: even lower A_V/N_H from BSD and $a_b = 20$ μm, again to consume the available mass.

data, to the extent that their infrared–ultraviolet extinction contributions remain undetectable (it is not possible to hide particles at the small size end because there is a constraint from the ultraviolet extinction; see Paper I). The fraction of the silicate mass in particles larger than 3 μm is 0%, 33%, and 65% for the three models, respectively. The corresponding numbers for graphite are 0%, 35%, and 55%. The fraction of the total extinction at V contributed by these particles is 0%, 1.1%, and 1.3%, and so they are well "hidden" (low cross section per unit volume in the observable range).

The mass distributions at large sizes are not unique since they are unconstrained by the extinction data. However, it is important to note that for the two mass-conserving mass distributions there is not a smooth and monotonic transition from the intermediate- to the large-size particles; instead the mass distributions have become rather bimodal. Although there is a smooth default through the 1–3 μm size range, the MEM analysis demonstrates that there is a real deficit of particles there. *Particles in this size range would produce a detectable effect on the observed extinction curve, basically a flattening of the near-infrared portion, a robust effect rather independent of what grain materials are being used.* Consequently their numbers (mass) can be constrained in a significant way. The MEM analysis then puts the extra mass in even larger particles that are well hidden.

How such mass distributions could have evolved from those in Figures 1 and 2 is an interesting matter for further study (the number distribution is of course steeply falling to large sizes). Clearly the size increase is so large that accretion would be irrelevant, leaving aggregation as the favored process. Distinct aggregates of pure silicate and graphite seem unlikely (Mathis & Whiffen 1989), but as mentioned the qualitative shape of the mass distributions should not change. It should also be emphasized that the aggregation envisaged here involves so much mass that all particles, including the largest ones in the original distribution, must be involved. This is to be contrasted with the modest grain growth needed to explain changes in R_V and λ_{max} (§ 2.2), which (in the extreme) might involve no large-particle–large-particle aggregation.

4.1. *Evolution of the Surface Area*

Cardelli (1988) has described how the evolution of the grain size distribution with increasing R_V can affect equilibrium molecular abundances, through an increase in penetrating ultraviolet radiation causing enhanced photodestruction, and, in the case of molecules like H_2, through a decreased grain surface area (Σ: units cm^2 per H nucleon) available for molecule formation. Snow (1983) made a simple estimate that toward ρ Oph the surface area had decreased by a factor of 2–3 compared to the diffuse interstellar medium, which might explain the unusually low H_2 abundance in this dark cloud line of sight; Cardelli's analysis extends and supports this.

With our detailed derived size distributions, we can calculate how Σ evolves. For $R_V = 3.1$, $\Sigma = 6.0 \times 10^{-21}$ cm^2; because the surface area distribution is close to a power law $s(a) \propto a^{-1.5}$ (Paper I), most of the surface area is contributed by small grains (the precise area is sensitive to the smallest bin size chosen and the uncertain shape of the size distribution there; the mass, on the other hand, tends to be in large grains). Thus when the small particles disappear with increasing R_V, the surface area decreases. For the models in § 2 with the same amount of material but $R_V = 2.7$, 3.1, 4.2, and 5.3 we find $\Sigma = 6.7$, 6.0, 4.3, and 2.9×10^{-21} cm^2, respectively.

The first ρ Oph dust model discussed above, with the SvS value of A_V/N_H and $a_b = 0.2$ μm, has less than the standard amount of material and $\Sigma = 2.9 \times 10^{-21}$ cm^2. Adding the large particles to use up the available mass is accompanied by a slight rearrangement of the rest of the mass distribution (there are somewhat fewer small particles needed because of the neutral extinction contribution of the added large particles), actually decreasing the surface area of the entire distribution ($\Sigma = 2.6 \times 10^{-21}$ cm^2). With the even lower BSD value of A_V/N_H, Σ would fall to 1.7×10^{-21} cm^2. Therefore, our models provide quantitative support for analyses such as by Cardelli (1988). A more refined treatment would question as well whether the efficiency of molecule formation is also a function of grain size and composition.

5. POTENTIAL OBSERVATIONAL CONSTRAINTS ON LARGE PARTICLES

5.1. *Scattering from the Near-Infrared to Far-Ultraviolet*

From the MEM mass distributions we can calculate the scattering properties of the interstellar grains. Two commonly used diagnostics are ω, the albedo, and g, the asymmetry parameter of the phase function. In Paper I we showed how both ω and g in the near-infrared were higher for the MEM mass distribution for $R_V = 3.1$ compared to the Mathis et al. (1977) size distribution, which does not have any particles larger than 0.25 μm. Results for the mass distributions shown in Figure 1 (for $R_V = 2.7$, 3.1, 4.2, and 5.3) and Figure 2 (for $R_V = 3.1$ but $a_b = 10$ μm) are shown in Figure 7. The main systematic effect is an overall increase in ω and g as R_V is increased; this arises because the relative number of larger particles increases with R_V (Fig. 1). The other effect concerns the two solutions for $R_V = 3.1$ shown in Figure 2. The case with $a_b = 10$ μm has a greater relative number of large particles, which raises ω and g in the near-infrared (the fractional variation in g is much larger than that in ω); however, there is a slight decrease through the optical and ultraviolet. This is reinforced in Figure 8, which shows results for the ρ Oph models in Figure 6. Unfortunately, ω and g are not very precisely known over the entire wavelength range even for $R_V = 3.1$ (Paper I), and environmental changes (with R_V) are undocumented. Investigations in the near-infrared would appear to be the most discriminating.

5.2. *10 and 20 Micron Silicate Feature*

Some of the particles in the extended mass distributions are large even compared to a wavelength of 10 μm, and so we investigated the mid-infrared, which includes the 10 and 20 μm silicate features. We used the optical constants determined according to Draine & Lee (1984; see also Draine 1985, 1987) both for silicate and graphite. For models with graphite grains larger than 1 μm the suggested infrared dielectric function becomes sensitive to size and temperature, whereas we used throughout that for $a = 0.1$ μm and 25 K. Although the above MEM analysis to obtain the mass distributions is unaffected, the subsequent detailed predictions of the infrared behavior would be.

The extinction τ/N_H is shown in Figure 9 for the mass distributions in Figure 1. Since the total mass of each com-

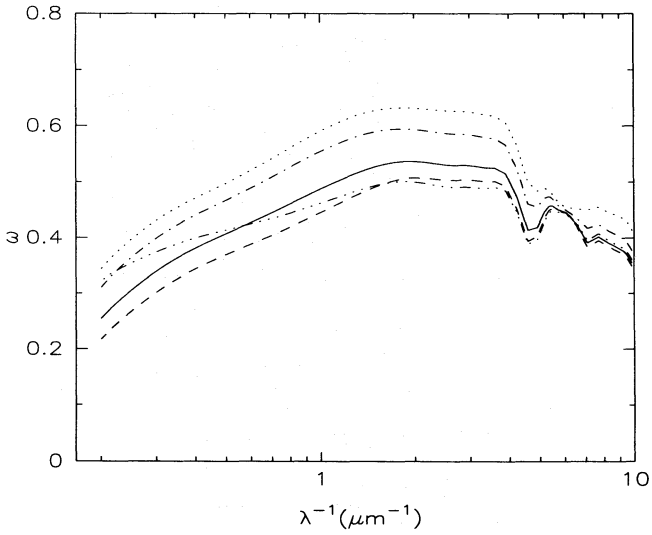

FIG. 7a

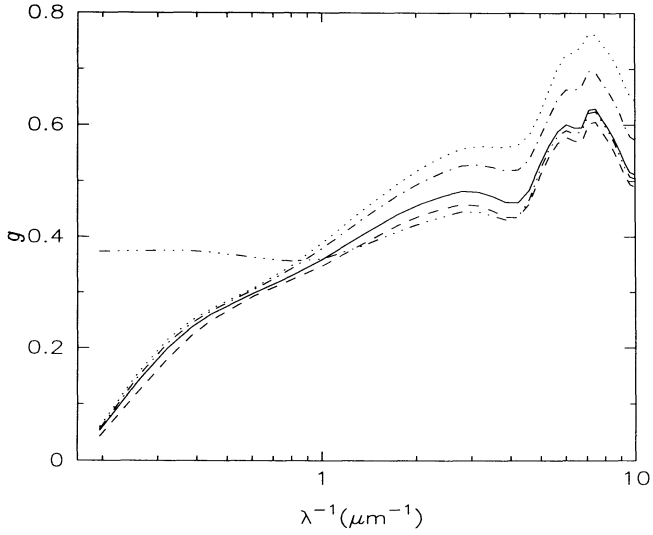

FIG. 7b

FIG. 7.—Scattering parameters from the near infrared to ultraviolet predicted for different mass distributions in Fig. 1 (same line types) and the $a_b = 10$ μm model in Fig. 2 (*triple-dot dashed curve*). (*a*) albedo (ω); (*b*) asymmetry parameter (g).

ponent is the same despite changes in R_V, and a_b is small (limiting the numbers of large grains), the silicate features (τ_{10} and τ_{20}) are virtually the same (see also § 6; there is also little change in the underlying continuum against which τ_{10} is often measured). The extinction in the near-infrared is higher for larger values of R_V. Note that τ_{10}/A_V would decrease slightly with increasing R_V because of the increased A_V/N_H. The extinction for the $a_b = 10$ μm model in Figure 2 is also included; although there are relatively more large silicate particles, the magnitude of the increase is too small to have an effect near 10 μm.

Figure 10 shows comparable results for the mass distributions shown in Figure 6 for ρ Oph. The solid curve, for the small a_b model that uses less mass, is more or less a scaled-down version of the $R_V = 4.2$ curve in Figure 9. The two models with the larger values of a_b (*dashed and dotted curves*) use up the same (all of the) mass as in Figure 1, but τ_{10}/N_H is lower (by factors 0.80 and 0.46, respectively) because there are now so many large particles in which the 10 μm extinction is saturated. The 20 μm extinction is less saturated, and so the ratio τ_{20}/τ_{10} increases.

While these are substantial changes, at the moment neither the silicate band strengths (silicate dielectric function through the features), their ratio, nor observations of τ_{10}/A_V are known sufficiently accurately to make a definitive study of evolutionary effects. For this reason, these parameters are not used as constraints on the MEM solutions at this time.

We also calculated ω (and g) in this region for the various models. The albedo at 10 μm is almost zero (almost pure absorption) for most cases, being a bit higher for larger R_V (see solid curve in Fig. 11 for $R_V \sim 4.2$). The albedo for the ρ Oph models is shown in Figure 11. For the mass distributions with large particles ω is enhanced at the features;

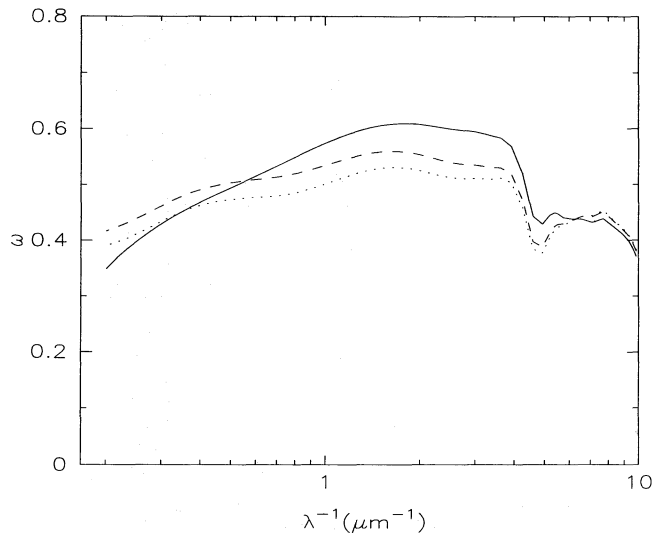

FIG. 8a

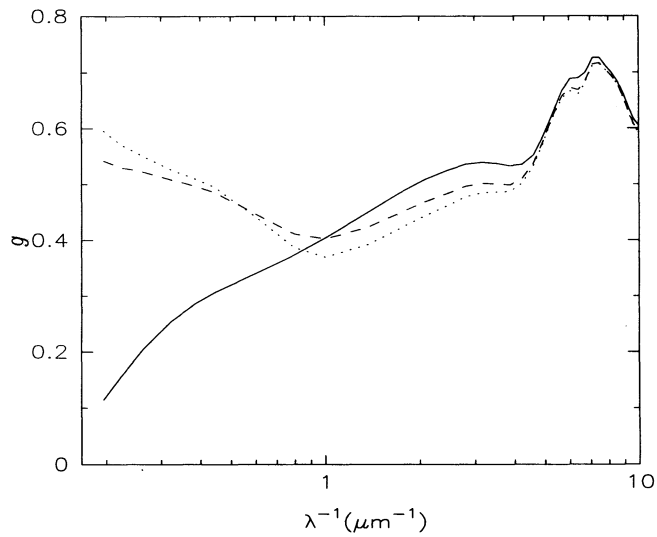

FIG. 8b

FIG. 8.—Same as Fig. 7 except for mass distributions for ρ Oph in Fig. 6 (same line types)

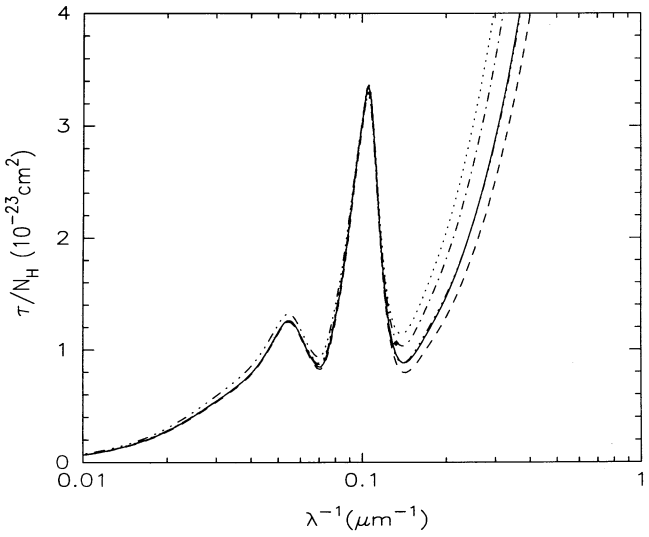

FIG. 9.—10 and 20 μm silicate features and near infrared continuum extinction for the mass distributions in Fig. 1 (same line types) and the $a_b = 10$ μm model in Fig. 2 (*triple-dot dashed curve*).

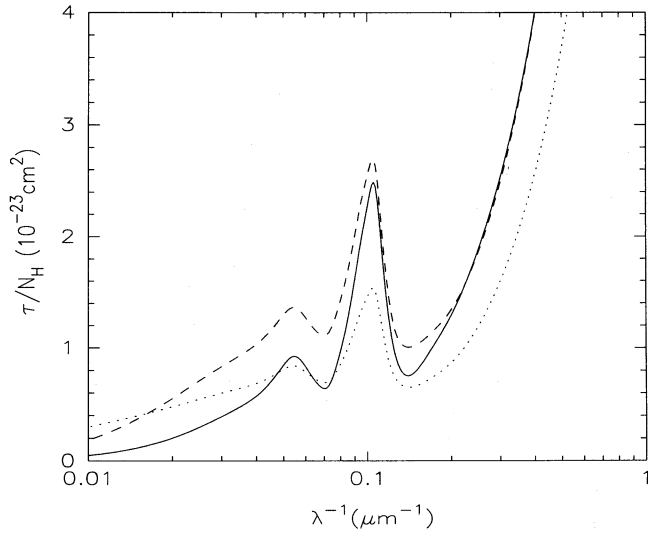

FIG. 10.—Same as Fig. 9 except for mass distributions for ρ Oph in Fig. 6 (same line types).

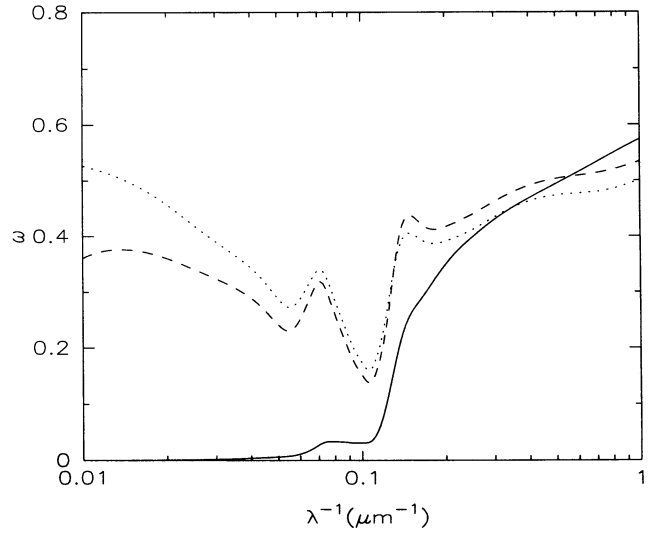

FIG. 11.—Infrared albedo calculated for mass distributions for ρ Oph in Fig. 6 (same line types).

but more dramatic is the increase in ω into the far-infrared. Observable consequences (e.g., scattered light is polarized) are probably limited since the total scattering optical depth is small.

We have not calculated the infrared emission that depends on the incident radiation field as well as the size distribution. It can be noted that the large particles will be relatively cooler, with potential enhancements in the far-infrared and submillimeter emission compared to models without these large particles.

6. KRAMERS-KRONIG APPROACH TO THE DUST TO GAS MASS RATIO

It is clear from the above that A_V/N_H is not necessarily the best measure of the dust to gas ratio. Purcell (1969) has suggested a potentially powerful alternative based on application of the Kramers-Kronig relations to the interstellar extinction curve. This approach is certainly instructive, but it is not without its limitations in practice.

The basic integral relation for a single grain composition is (Purcell 1969; Martin 1978; Bohren & Huffman 1983)

$$\int_0^\infty \frac{C}{Vw}\, d\ln w = \pi^2 f = \pi^2 \frac{\epsilon_0 - 1}{L(\epsilon_0 - 1) + 1}\ , \qquad (3)$$

where $w \equiv \lambda^{-1}$, V is the volume of grains involved, C is the total extinction cross section produced by the grains, and f is a factor near unity. For spheroidal shapes, the right-hand expression for f holds, with ϵ_0 the static dielectric constant of the grain material and L a shape- and orientation-dependent depolarization factor ($\frac{1}{3}$ for spheres used here). In theoretical simulations this integral equation can be evaluated self-consistently only when the cross sections are derived from a complex dielectric function which itself obeys the Kramers-Kronig relations. Such is the case for the component materials we have been using above.

In Figure 12 we show the integrand (logarithmic form) for the different silicate mass distributions in Figure 1 (see also Martin & Rouleau 1991). Although the wavelength dependence of extinction (and the mix of absorption and

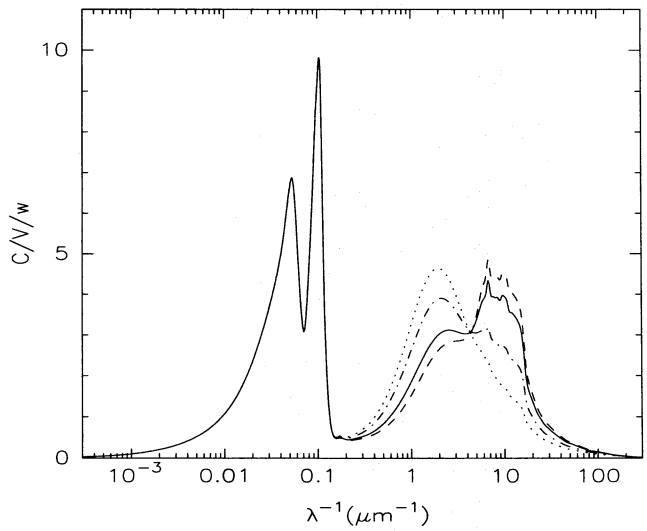

FIG. 12.—Extinction cross sections of silicate per unit volume divided by the wavenumber w ($C/V/w$ is dimensionless), the integrand of the Kramers-Kronig relation in eq. (3). The four curves are for the silicate mass distributions in Fig. 1 (same line types); the areas under the curves are equal.

scattering) changes dramatically in the optical and ultraviolet, the area under each curve is the same ($f = 2.34$); we have verified equation (3) numerically to high precision (analytic continuations are used to low and high wavenumbers; the contributions are negligible). The infrared behavior for the four models is the same; for the size parameters encountered here the extinction (actually electric dipole absorption) scales directly with the volume. The portion of the integral in the observable range 0.2–10 μm^{-1} is 0.36, 0.38, 0.41, and 0.44 for $R_V = 2.7$, 3.1, 4.2, and 5.3, respectively. About half of the integral is contained in the range 0–0.2 μm^{-1}. Purcell (1969) has suggested that in cases like this with fairly isolated infrared resonances one could use the infrared dielectric function (lower than that at zero frequency) to approximate f (one obtains a lower value) for use in equation (3) with the remaining optical-ultraviolet portion of the integral. While not exact, it appears to be not too bad for these particular silicate models, but it cannot be generalized to cases with an abundance of large particles or to materials like graphite.

Figure 13 gives the corresponding information for the graphite component ($f = 3$). The portion of the integral in the observable range 0.2–10 μm^{-1} is 0.66, 0.66, 0.67, and 0.67 for $R_V = 2.7$, 3.1, 4.2, and 5.3, respectively. Compared to silicate, much less of the graphite material is missed in this census (in the context of the carbon budget, carbon material is not overly "wasted"). Despite the constant mass (volume), a slight change can be seen in the vicinity of the infrared peak near 40 μm. The peak arises for the case with electric vector parallel to the c-axis, sitting on top of a smoothly falling continuum for the case with electric vector perpendicular to the c-axis (Draine & Lee 1984). The change arises in the perpendicular case, which has a significant magnetic dipole absorption contribution for large particles (scales as a^5 rather than a^3 for electric dipole absorption).

Jura (1980) has commented that the extinction depends only on the mass column density if the wavelength is sufficiently long. In support of his argument for aggregation he suggested using the L passband (3.6 μm or 0.26 μm^{-1}). However, these figures clearly show that this suggestion is not appropriate at all for either silicate or graphite grain components: scattering is not negligible because of the presence of large-sized particles required to fit the extinction curve, and so the value of A_L does change with the mass *distribution* even for constant mass. See also the upper two curves (*solid and dashed*) in Figure 10 for ρ Oph, which are for different masses yet have the same L-band extinction, and the upper and lower curves (*dashed and dotted*), which are for the same mass yet have different L-band extinction. In any case, measuring A_L is not without difficulty, since A_L is a small number that depends critically on precise knowledge of the extrapolation of the extinction curve to zero frequency. While there appears to be a common behavior of the frequency dependence of near-infrared extinction, like a power law, independent of R_V (CCM; Martin & Whittet 1990), nevertheless A_L is still prone to significant fractional uncertainty from even small observational errors or departures from a common power law.

For the particular set of models in Figure 12, the silicate curves cross near 4.4 μm^{-1}, suggesting this as a more robust place to measure the dust to gas mass ratio. But for graphite (Fig. 13) the curves cross near 2.0 μm^{-1} instead, showing that there is nothing general in this approach (in combination, the curves cross near 2.8 μm^{-1}, close to the U rather than the V passband; see Fig. 14).

Applying this Kramers-Kronig approach to obtain the dust to gas ratio from the observed extinction requires some manipulation to the final form

$$\int_0^\infty \frac{A}{N_H w}\, d\ln w = 1.086\pi^2 m_H \sum \frac{f}{s_d}\frac{M_d}{M_H}, \qquad (4)$$

where s_d is the grain density (3.3 g cm^{-3} for silicate and 2.26 g cm^{-3} for graphite) and M_d is the column density of dust for hydrogen column density $M_H = m_H N_H$. The integrand is plotted in Figure 14 for the models in Figure 1. Note again the constancy in the mid-infrared, since the models have equal mass and few large particles. Again we have verified equation (4) numerically.

Consider finding the integrand from observations rather than from theory. It is not sufficient to have a normalized

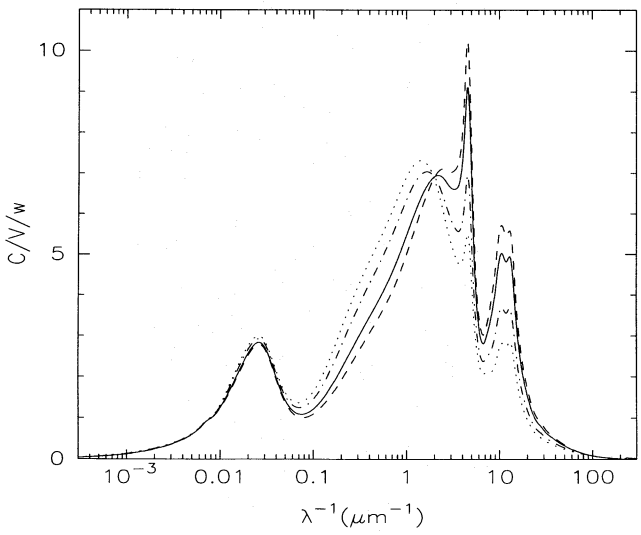

FIG. 13.—Like Fig. 12 but for the graphite component

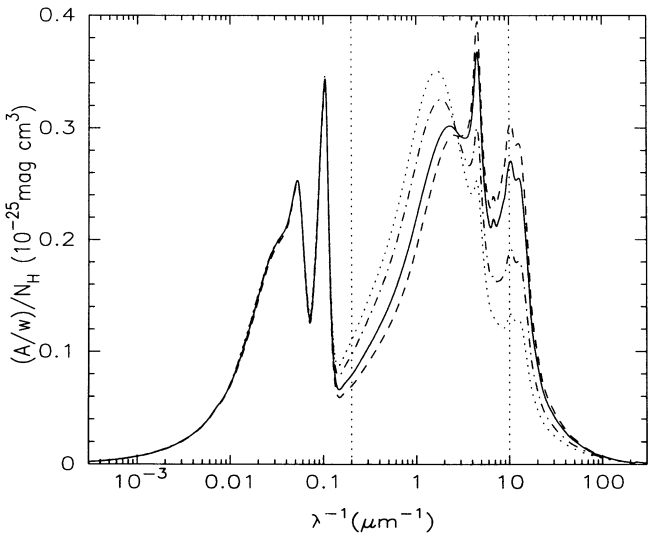

FIG. 14.—Extinction per unit H column density divided by the wavenumber w, $A/N_H/w$ (the units emphasize that this is a basic measure of grain volume), the integrand of the Kramers-Kronig relation in eq. (4). The four curves are for the mass distributions in Fig. 1 (same line types); the areas under the curves are equal. Vertical dotted lines mark the range 0.2–10 μm^{-1} within which observations are available.

extinction curve, like $A/E(B-V)$ or A/A_V. The scale of A/N_H is required, for example, A_V/N_H from equation (1) when $R_V = 3.1$. Even when the integral is constant (constant mass), we have seen how A_V/N_H can change with the shape of the mass distribution. Equation (4) essentially tells us how to transform A_V/N_H into M_d/M_H.

A major limitation in practice, even for $R_V = 3.1$, is the incomplete wavelength coverage of the observations. It is useful to use the integrand predicted self-consistently from our fitted mass distributions (Fig. 14) to estimate what fraction of the integral can be observed. The fraction in the optical wavelength range used by Purcell (0.44–3 μm^{-1}) is 0.26, 0.28, 0.33, and 0.36 for the $R_V = 2.7$, 3.1, 4.2, and 5.3, respectively. If we increase the wavelength range to 0.2–10 μm^{-1} (the range used to derive the mass distributions from the extinction curve and marked by the vertical dotted lines in Fig. 14), then the fraction grows to 0.52, 0.53, 0.55, and 0.57, respectively. It is perhaps encouraging that this fraction is so robust; as R_V increases the increased contribution to the integral in the near-infrared and visual is offset by the decreased contribution from the observable ultraviolet (Fig. 14).

Another source of uncertainty is that f/s_d is not constant for the different compositions (0.71 and 1.33 for silicate and graphite spheres, respectively). Even if this ratio were constant and the total dust to gas mass ratio could be determined, the relative amounts of silicate and graphite could not be found from this single equation (additional information would be required, e.g., the albedo, or τ_{10}/A_V, or assume silicate contribution is known from cosmic abundances and depletion and then derive carbon content).

Figure 15 shows the same information for the ρ Oph models of Figure 6. Compared to the solid curve, the dashed curve encloses more area (in the ratio 1:0.7) because of the additional contribution of the large particles (both silicate and graphite) in the infrared (0–0.2 μm^{-1}). Compared to the dashed curve, the dotted curve encloses the same area (same mass in models) but has an additional contribution from large particles in the infrared to compensate for the lower mass of small particles causing extinction in the optical and ultraviolet.

While extraction of the precise dust to gas ratio from equation (4) is difficult, differential comparisons should be

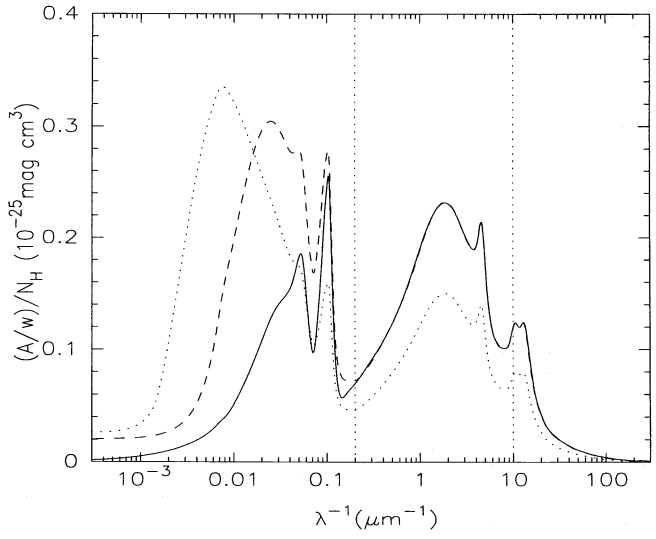

FIG. 15.—Same as Fig. 14 except toward ρ Oph (Fig. 6, same line types)

valuable. The curves in the range 0.2–10 μm^{-1} represent the data (which are fitted accurately by the models). For the solid and dashed curves in Figure 15, this portion of the integral is 0.61×10^{-25} mag cm^{-3} to be compared to the same portion from the diffuse medium ($R_V = 3.1$) curve in Figure 14, 0.85×10^{-25} mag cm^{-3}; the ratio is 0.72. For the dotted curve the ratio is only 0.47. Assuming the observations are correct, *this analysis provides a strong argument that a significantly lower dust to gas (volume) ratio is needed to explain the near-infrared to ultraviolet extinction along the line of sight to* ρ Oph. This conclusion is consistent with but more directly rooted in theory—and hence more robust—than the consideration of A_V/N_H alone. We feel that arguments based on the "integrated extinction" $\int A/A_V\, dw$ (CCM) are less reliable.

This does not by itself imply aggregation. However, if it is demanded independently that the same amount of mass be in grains, the dashed and dotted curves in Figure 15 show how the effect of this material must be hidden: in the infrared. The MEM analysis shows quantitatively the significant mass in large particles that has to be explained by an aggregation theory.

Let us return finally to the crisis that would be posed by a low cosmic C/H ratio (§ 2.3). Our specific models have shown that graphite grains account for a fraction 0.55 of the sum (of effectively fV) on the right-hand side of equation (4) and hence the same fraction of the integrated extinction. The important contribution of graphite to extinction in the optical and ultraviolet can be seen in Figures 1*b* and 2*b* in Paper I. Integrated over the observed range 0.2–10 μm^{-1} graphite contributes a fraction of only 0.36. Nevertheless, of the fraction 0.52–0.57 that can actually be observed over this range, graphite accounts for 69%–65%. As discussed in § 2.3, redistributing some carbon in the form of amorphous carbon and restricting the size distribution through a_b can ease the carbon budget by a factor 0.77 (from C/H $\sim$ 310 ppM to 240 ppM) while maintaining the extinction (or fV). But lowering the carbon available for dust further from 240 ppM to only 100 ppM is very serious, presumably now lowering fV and removing a large visual wavelength contribution to the integrated extinction at the very least. One would need another grain contribution with observable integrated extinction comparable to that from silicates (and comparable fV as well, certainly more than half), which is a significant challenge.

One might wonder whether fluffy aggregates might cause more efficient extinction from a given amount of material, thus lowering the dust to gas ratio (in the case of a C/H crisis, maximizing fV per carbon atom). A specific example mentioned in § 2.3 suggests that this is not an easy fix: the composite fluffy grain model of Mathis & Whiffen (1989), using the Bruggeman mixing rule, in fact uses about the same amount of silicate and carbon material as the models with separate silicate and carbon particles. More generally, how is the increase in volume in a fluffy particle offset by a lowering of the effective dielectric function? An overall answer might be gleaned from equation (4), if one uses an effective medium theory (valid at low frequencies) to evaluate the right-hand side, basically the product fV. The Maxwell Garnett rule with vacuum matrix for spheres (Bohren & Huffman 1983), for example, predicts no enhancement, while others like the Bruggeman rule probably overestimate the enhancement (Rouleau & Martin 1993). Note also that any enhancement in fV (right-hand

side of eq. [4]) associated with a high dielectric function (high f) would also be associated with the same magnitude of enhancement in extinction in the infrared (unobserved at low frequencies), which would increase the left-hand side correspondingly. Useful constraints specifically on the material causing the visual extinction would in this case be difficult to extract.

7. SUMMARY

1. For $R_V = 2.7$, 3.1, 4.3, and 5.3, we have determined mass distributions of interstellar dust particles that fit the extinction curves and also give the maximum A_V/N_H for a fixed amount of material (the latter minimized for $R_V = 3.1$). The maximum A_V/N_H increases with R_V.

2. The amount of carbon used in the models with graphite is C/H = 310 ppM but could be reduced to perhaps 240 ppM with amorphous carbon. If the total cosmic (interstellar) abundance were as low as suggested by Galactic B stars (say 240 ppM) and the gas phase abundance is 140 ppM, there would be a real crisis for grain models attempting to explain both the average A_V/N_H and the albedo at visual wavelengths.

3. We emphasize that A_V/N_H is a more relevant (although imperfect) dust to gas indicator than $E(B-V)/N_H$. A plot of A_V/N_H versus R_V shows a rather large scatter for $R_V < 4.4$. Despite the observational errors, we concluded that at higher R_V the value of A_V/N_H is lower than average. This conclusion needs to be bolstered by observations on lines of sight sampling further distinct environments.

4. We have determined the mass distribution for the line of sight to ρ Oph for two different A_V/N_H values that are lower than the average. We have found that additional large particles are required to use up the available mass and that there is not a smooth or monotonic transition from the intermediate- to the large-size particles; instead the mass distributions have become rather bimodal. To produce a significant mass of such large particles by aggregation, all particles, including the largest ones in the original distribution, must be involved.

5. We have calculated how the total surface area of grains per H nucleon decreases with increasing R_V. This might help explain the unusually low H_2 abundance toward the ρ Oph cloud.

6. For the various mass distributions, scattering properties ω (the albedo) and g (asymmetry parameter of the phase function) have been calculated. There is an overall increase in ω and g as R_V is increased; the presence of large particles in a distribution is most clearly manifested as increased ω and g in the near-infrared.

7. Using the optical constants determined by Draine & Lee (1984), we have calculated the 10 and 20 μm silicate features (τ_{10}/N_H and τ_{20}/N_H) for various mass distributions. The silicate features are virtually the same for the various models with different R_V. But for cases like ρ Oph, where large particles are present, τ_{10}/N_H is lower and the ratio τ_{20}/τ_{10} increases.

8. We have carried out Kramers-Kronig integrals to show their potential relationship to a determination of the dust to gas ratio. We discuss why in practice finding the precise dust to gas ratio is difficult, but point out that differential comparisons should be valuable. For the case of ρ Oph, whose A_V/N_H is lower than average, the integral of the extinction curve in the range 0.2–10 μm^{-1} is lower than for the "standard" model for $R_V = 3.1$ (or $R_V = 4.2$ since this is rather independent of R_V). This analysis provides a strong argument for a significantly lower dust to gas ratio for "normal-sized" dust along the line of sight to ρ Oph; the missing material could be in larger grains that are harder to detect.

Note added in manuscript.—Many aspects of the cosmic carbon abundance, including what we have called the carbon crisis in § 2.3, have been discussed in a recent paper by Snow & Witt (1995). Tielens et al. (1996) provide a census of various interstellar grain components, agreeing with our bottom-line requirement for a substantial amount of carbon in interstellar grains—evidence for a low cosmic carbon abundance not withstanding.

We thank the referee, J. Cardelli, for helpful comments that have led to improvements in the manuscript. We appreciated receiving preprints of recent papers by J. Cardelli and J. Mathis. This work was supported by the Natural Sciences and Engineering Research Council of Canada.

REFERENCES

Bohlin, R. C., Savage, B. D., & Drake, J. F. 1978, ApJ, 224, 132 (BSD)
Bohren, C. F., & Huffman, D. R. 1983, Absorption and Scattering of Light by Small Particles (New York: Wiley-Interscience)
Cardelli, J. A. 1988, ApJ, 335, 177
Cardelli, J. A., Clayton, G. C., & Mathis, J. S. 1989, ApJ, 345, 245 (CCM)
Cardelli, J. A., Meyer, D. M., Jura, M., & Savage, B. D. 1996, ApJ, submitted
Carrasco, L., Strom, S. E., & Strom, K. M. 1973, ApJ, 182, 95
Clayton, G. C., & Mathis, J. S. 1988, ApJ, 327, 911
Chlewicki, G., & Greenberg, J. M. 1990, ApJ, 365, 230
de Boer, K. S., Lenhart, H., van der Hucht, K. A., Kamperman, T. M., Kondo, Y., & Bruhweiler, F. C. 1986, A&A, 157, 119
Diplas, A., & Savage, B. D. 1994a, ApJS, 93, 211
———. 1994b, ApJ, 427, 274
Draine, B. T. 1985, ApJS, 57, 587
———. 1987, Princeton Obs. preprint, POP-213
Draine, B. T., & Lee, H.-M. 1984, ApJ, 285, 89
Duley, W. W., Jones, A. P., & Williams, D. A. 1989, MNRAS, 236, 709
Fitzpatrick, E. L., & Massa, D. 1990, ApJS, 72, 163
Green, J. C., Snow, T. P., Cook, T. A., Cash, W. C., & Poplawski, O. 1992, ApJ, 395, 289
Grevesse, N., Lambert, D. L., Sauval, D. L., van Dishoeck, E. F., Farmer, C. B., & Norton, R. H. 1991, A&A, 242, 488
Grevesse, N., & Noels, A. 1993, in Origin and Evolution of the Elements, ed. N. Prantzos, E. Vangioni-Flam, & M. Cassé (Cambridge: Cambridge Univ. Press), 15
Hollenbach, D. J., Takahashi, T., & Tielens, A. G. G. M. 1991, ApJ, 377, 192
Jaffe, D. T., Zhou, S., Howe, J. E., Herrmann, F., Madden, S. C., Poglitsch, A., van der Werf, P. P., & Stacey, G. J. 1994, ApJ, 436, 203
Jenniskens, P., Baratta, G. A., Kouchi, A., de Groot, M. S., Greenberg, J. M., & Strazzula, G. 1993, A&A, 273, 583
Jura, M. 1980, ApJ, 235, 63
Kim, S.-H., & Martin, P. G. 1994, ApJ, 431, 783
———. 1995, ApJ, 444, 293
Kim, S.-H., Martin, P. G., & Hendry, P. D. 1994, ApJ, 422, 164 (Paper I)
Lacy, J. H., Knacke, T. R., Geballe, T. R., & Tokunaga, A. T. 1994, ApJ, 428, L69
Martin, P. G. 1978, Cosmic Dust (Oxford: Oxford Univ. Press), 194
———. 1995, ApJ, 445, L63
Martin, P. G., & Rouleau, F. 1991, in Extreme Ultraviolet Astronomy, ed. R. F. Malina & S. Bowyer (Oxford: Pergamon), 341
Martin, P. G., & Whittet, D. C. B. 1990, ApJ, 357, 113
Mathis, J. S. 1996, in ASP Conf. Ser., Polarimetry of the Interstellar Medium, ed. W. G. Roberge & D. C. B. Whittet (San Francisco: ASP), in press

Mathis, J. S., Rumpl, W., & Nordsieck, K. H. 1977, ApJ, 217, 425
Mathis, J. S., & Whiffen, G. 1989, ApJ, 341, 808
Meyer, D. M., Jura, M., Hawkins, I., & Cardelli, J. A. 1994, ApJ, 437, L59
Purcell, E., M. 1969, ApJ, 158, 433
Rouleau, F., & Martin, P. G. 1993, unpublished
Rowan-Robinson, M. 1992, MNRAS, 258, 787
Savage, B. D., Bohlin, R. C., Drake, J. F., & Budich, W. 1977, ApJ, 216, 291
Savage, B. D., & Massa, D. 1987, ApJ, 314, 380
Serkowski, K. 1968, ApJ, 154, 115
Serkowski, K., Mathewson, D. S., & Ford, V. L. 1975, ApJ, 196, 261
Shull, J. M., & van Steenberg, M. E. 1985, ApJ, 294, 599 (SvS)
Snow, T. P. 1983, ApJ, 269, L57
Snow, T. P., & Jenkins, E. B. 1980, ApJ, 241, 161
Snow, T. P., & Witt, A. N. 1995, Science, 270 (5241), 1455
Sophia, U. J., Cardelli, J. A., & Savage, B. D. 1994, ApJ, 430, 650
Tielens, A. G. G. M., Wooden, D. H., Allamandola, L. J., Bregman, J., & Witteborn, F. C. 1996, ApJ, 461, 210
Vrba, F. J., Coyne, G. V., & Tapia, S. 1993, AJ, 105, 1010